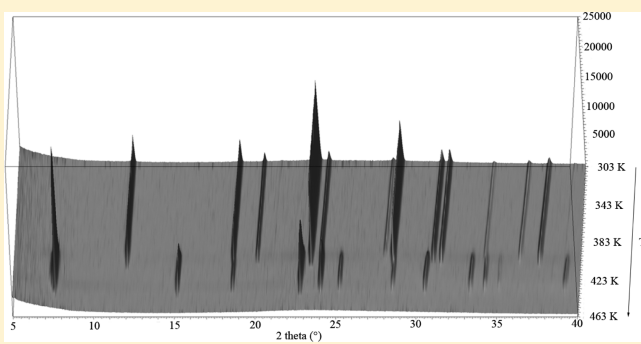


Crystal Polymorphism of Propylammonium Chloride and Structural Properties of Its Mixture with Water

Valentina Migliorati,[†] Paolo Ballirano,^{*,‡} Lorenzo Gontrani,^{†,§} Olga Russina,[†] and Ruggero Caminiti[†][†]Dipartimento di Chimica, Sapienza Università di Roma, Piazzale Aldo Moro 5, I-00185 Roma, Italy[‡]Dipartimento di Scienze della Terra, Sapienza Università di Roma, Piazzale Aldo Moro 5, I-00185 Roma, Italy[§]CNR-Istituto di Struttura della Materia, Area della Ricerca di Roma 2, Tor Vergata, Via del Fosso del Cavaliere 100, I-00133 Roma, Italy**S** Supporting Information

ABSTRACT: The thermal behavior of propylammonium chloride (PAC) has been investigated by parallel beam X-ray powder diffraction in the 303–463 K thermal range. A polymorphic transition has been observed at 403 K, whereas the melting process starts at 438 K. The low-temperature (LT) polymorph is tetragonal, $P4/n$ or $P4/nmm$, and $a = 6.2429(2)$ Å, $c = 7.3830(3)$ Å, and $Z = 2$. Thermal expansion is isotropic as the N···Cl interactions have components along the three crystallographic axes. At the transition temperature, a high-temperature (HT) polymorph was observed, with candidate space groups $P23$, $Pm\bar{3}$, $P432$, $P\bar{4}3m$, and $Pm\bar{3}m$ and cell parameter $a = 11.715(3)$ Å, consistent with $Z = 12$. This phase has features reminiscent of those of plastic phases of molecular crystals. The structural properties of a PAC/water mixture at ambient conditions were also studied by using an integrated approach, which combines X-ray diffraction measurements and molecular dynamics simulations carried out with the SPC/E and TIPSP water models. By using a Cl–water Lennard-Jones parameter previously refined for a similar system, a very good agreement between the theoretical and experimental diffraction patterns was obtained, especially in the case of the TIPSP simulation. A complex structural behavior has been highlighted, in which cations and anions do not possess a completely closed hydration shell of their own, but rather “solvent-shared ion pairs” are formed, where one or more water molecules act as a bridge between the chloride and propylammonium ions.



INTRODUCTION

In the last decades, a classical subject of physics and chemistry such as the structure and dynamics of molten salts, e.g., liquids constituted solely by ions, has attracted a considerable amount of interest. Among the several families of molten organic salts, alkylammonium chlorides, with general formula $C_nH_{2n+1}NH_3X$, are a particularly interesting class of compounds as it is possible to tailor the volume and shape of the organic cation by introducing different hydrocarbon chains.¹ Moreover, these materials have found wide application, for example, as reagents in organic and analytical chemistry and in electrochemistry as supporting electrolytes.¹

Despite their numerous applications, a fundamental understanding of the complex network of interactions that are built up in these compounds is still lacking. Among the various issues needing a deeper understanding, there are the crystal polymorphism of solid alkylammonium halides and their behavior in the mixture with other solvents such as water.²

In a recent work by this research group, the temperature dependence of an ethylammonium chloride (EAC) structure has been investigated by *in situ* laboratory parallel-beam X-ray powder diffraction.² A polymorphic transition, with a

reconstructive character, from a monoclinic low-temperature (LT) phase to a tetragonal high-temperature (HT) phase has been observed at 358 K. The thermal expansion of both polymorphs has been found to be small and anisotropic as a consequence of their organization through an anisotropic interaction network. Moreover, the HT phase (possible space group $P4/n$ or $P4/nmm$, $a = 5.05$ Å, $c = 9.99$ Å) was shown to have an excess volume of ca. 11% as compared to the LT one. The structural properties of an EAC/water mixture have also been studied by combining X-ray diffraction measurements and classical molecular dynamics (MD) simulations.² By refining a single interaction potential, a very good agreement between the theoretical and experimental diffraction patterns was obtained. A complex structural behavior has been highlighted, in which cations and anions do not possess a completely closed hydration shell of their own and strong cation–anion and water–water correlations are present.

Received: July 18, 2011**Revised:** September 5, 2011**Published:** September 07, 2011

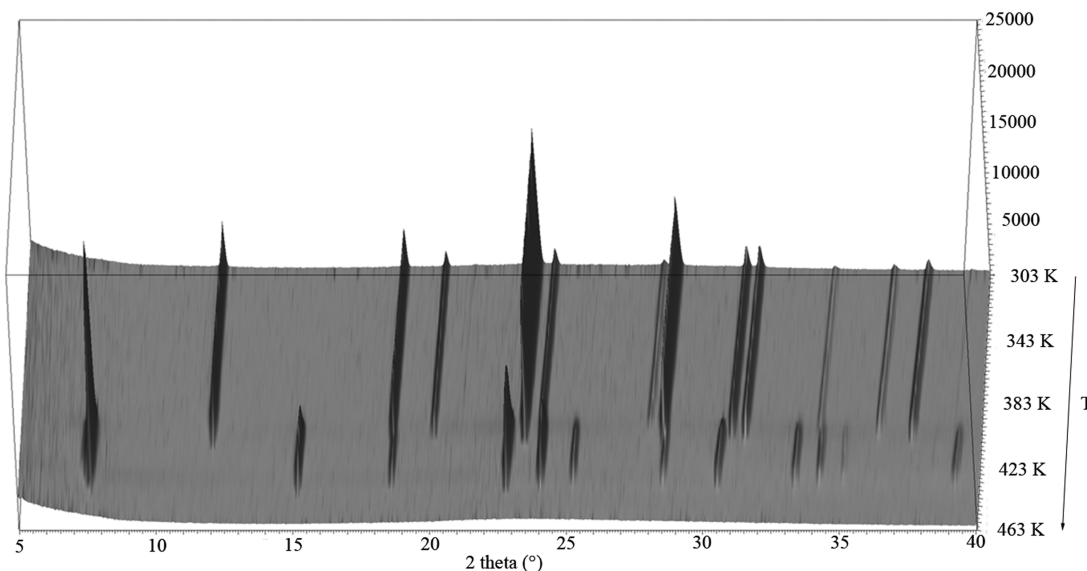


Figure 1. Magnified view ($5\text{--}40^\circ 2\theta$) of the full data set of the heating cycle of the title compound.

The combination of theoretical and experimental techniques has been found to be essential to gain accurate structural information on the EAC/water mixture, and this is not surprising since the study of the structural and dynamic properties of disordered systems, such as alkylammonium chlorides/water mixtures, is a complex task, and it is very difficult to obtain accurate information when using a single method of investigation.

In the framework of a broader investigation of this class of materials, we have used here the powerful combined approach previously adopted for EAC to study the thermal and structural properties of propylammonium chloride (PAC) and its mixture with water. To the best of our knowledge, no investigation has been carried out until now on mixtures of water and PAC. As far as the crystal polymorphism of PAC is concerned, PAC has been shown to possess two polymorphs.^{3,4} At RT isostructurality among propylammonium halides has been reported. The structure has tetragonal symmetry, e.g., $P4/nmm$, $a = 6.220(5)$ Å, $c = 7.377(8)$ Å, with two $C_3H_7NH_3X$ ($X = \text{chloride, iodide, and bromide}$) molecules per unit cell. The authors reported the occurrence of rotational or orientational disorder of the cations. However, a structural description consisting of fractional coordinates, displacement parameters, and associated standard deviations was not presented in full. At cryogenic temperatures, a monoclinic polymorph was found, e.g., $C2/m$, $a = 9.06(8)$ Å, $b = 8.58(8)$ Å, $c = 7.34(10)$ Å, $\beta = 98(2)^\circ$, the a axis of the monoclinic cell corresponding to [110], the b axis to [1 $\bar{1}$ 0], and the c axis to [001] of the RT tetragonal cell. The transition was attributed by the fixing of the positions of the cations in the (1 $\bar{1}$ 0) planes of the RT structure.

Therefore, the aim of the present paper is 2-fold: first to provide the crystallographic data required for a complete understanding of the structural modifications occurring during heating of PAC from RT to the melting point; second, to study the structural properties of a PAC/water mixture, by combining fully atomistic MD simulations and high-energy X-ray diffraction experiments. One important issue that will be addressed is whether the Lennard-Jones parameter for the Cl–water interaction previously optimized for EAC² is able to correctly describe the structural properties also of the PAC/water mixture.

Moreover, we will evaluate the performances of two of the most widely used water models present in the literature, namely, the SPC/E⁵ and TIPSP⁶, in providing a reliable description of the PAC/water mixture.

■ METHODS

X-ray Powder Diffraction Measurements. Powder of the title compound was loaded and packed in a 0.7 mm diameter borosilicate-glass capillary that was subsequently sealed. The sample, Aldrich 242543, was used without any further purification. The capillary was glued to a 1.2 mm diameter Al_2O_3 tube by means of a high-purity alumina ceramic (Resbond 989). The capillary/tube assembly was subsequently aligned onto a standard goniometer head, and diffraction data were collected on a parallel-beam Bruker AXS D8 Advance, operating in transmission in $\theta\text{--}\theta$ geometry. The instrument is fitted with a PSD VÄNTEC-1 detector set to a $6^\circ 2\theta$ aperture and with a prototype of capillary heating chamber.^{7–11} Data were measured in the $5\text{--}90^\circ 2\theta$ angular range, step size $0.0219^\circ 2\theta$, and 5 s counting time, using $\text{Cu K}\alpha$ radiation. Isothermal measurements were carried out in the 303–463 K thermal range with temperature steps of 5 K. A magnified view of the complete data set, consisting of 33 diffraction patterns, is shown in Figure 1.

A phase transition was observed at 403 K, whereas the melting process started at 438 K and was detected from an abrupt increase of the background counterbalanced by a strong general intensity reduction of the Bragg reflections.

Data Evaluation. For the LT polymorph, a LeBail fitting carried out with Topas 4.2¹² pointed to a tetragonal cell, with $a = 6.2429(2)$ Å and $c = 7.3830(3)$ Å. The reflection condition $0k0$ for $k = 2n$ and $hk0$ for $h + k = 2n$ is consistent with the extinction symbol $Pn\text{--}$. Therefore, candidate space groups were $P4/n$ or $P4/nmm$, confirming the findings of King and Lipscomb.³

Integrated intensities were extracted by the EXPO software¹³ and subsequently used for ab initio direct methods structure solution using the SIR97 software.¹⁴ Trials were performed in both possible space groups $P4/n$ and $P4/nmm$. However, the best final E-maps for each space group provided similar R values.

Cl was found at the origin, whereas N and C(1) were found at the site 0, 1/2, z. The remaining carbon atoms C(2) and C(3) were found to be rotationally disordered around the N–C(1) vector. Similarly to the HT polymorph of EAC,² considerations about site multiplicity and geometry of NH₃ seem to point to P4/n as the correct space group. However, no hydrogen atoms were included in the refinement because of the expected extended disorder. Therefore, because of the absence of clear indications, refinements of the structure were carried out in the centrosymmetric P4/nmm space group (origin choice 2). The derived fractional coordinates from direct methods were used as a starting value for the refinement of the structure with the GSAS suite of programs¹⁵ coupled with the EXPGUI graphical user interface.¹⁶ A structure refined at a given temperature was used as input for the subsequent temperature. Peak shape was modeled by a Pseudo-Voigt function modified to incorporate asymmetry.^{17,18} The Rietveld refinement procedure was the same as that reported for EAC.² N–C and C–C distances were restrained in the 1.47(1) and 1.54(1) Å ranges. Moreover, N–C–C and C–C–C bond angles were restrained using N–C (2.47(2) Å) and C–C (2.52(2) Å) pseudobonds. The statistical associated weight was set to 20. The restraint contribution to χ^2 never exceeded 1.2%, indicating a proper weighting scheme. The use of restraints has been proved to render more stable Rietveld refinements and to avoid convergence toward

Table 1. Miscellaneous Data of the Various Rietveld Refinements^a

R _p (%)	4.24–4.54
R _{wp} (%)	5.54–6.13
R _{F2}	13.87–16.28
χ^2	1.90–2.24
refined parameters	47 (30 background)
restraints	8
contribution of restraints to χ^2 (%)	0.6–1.2
J	1.150 (averaged)

^a Statistic indicators as defined by ref 21.

false minima.¹⁹ Isotropic displacement parameters were refined constraining those of the N and C atoms of the cation to be equal. Such simplification was adopted to reduce the number of refined parameters.

Texture occurrence was evaluated by means of a generalized spherical-harmonic description²⁰ up to the spherical harmonic order of eight, including eight refinable *l*, *m*, *n* terms (2,0,0; 4,0,0; 4,0,4; 6,0,0; 6,0,4; 8,0,0; 8,0,4; 8,0,8). As expected for a capillary mount, an almost complete absence of preferred orientation was observed as a result of calculated texture indices *J* close to one. During the final refinement cycles, the coefficients of the various *l*, *m*, *n* terms were kept fixed to the corresponding mean values, as calculated from the 21 diffraction patterns (corresponding to an average *J* = 1.1505). It is possible that a part of the limited correction has been required to compensate the absence of the hydrogen atoms from the refinements.

Miscellaneous data of the various refinements are reported in Table 1. An example of the Rietveld plots obtained for the diffraction pattern collected at 303 K is reported in Figure 2. CIF files were submitted as Supporting Information.

X-ray Scattering measurements. The molten salt PAC was dried in vacuum for about 48 h. The PAC/water mixture was then prepared by adding a weighted amount of freshly distilled water to a weighted amount of solid PAC in a round-bottomed flask, thus obtaining a PAC/water molar ratio of 1:6.51.

The choice of this molar ratio is motivated by the fact that we intend to compare the structural properties of the PAC/water mixture with those previously obtained for the mixture with water of the lower homologue (EAC).² By using this molar ratio, we have exactly the same ion concentration in the EAC/water and PAC/water mixture, and we can directly compare the diffraction patterns of the two samples. Moreover, we intend to study the PAC/water mixture for an intermediate concentration of water, where the water molecules are neither in deficiency nor in great excess as compared to the number of ion pairs. Since the hydration number of Cl⁻ in aqueous solution is 6 (vide infra), 6.51 water molecules are supposed to be enough to saturate the anion coordination sphere.

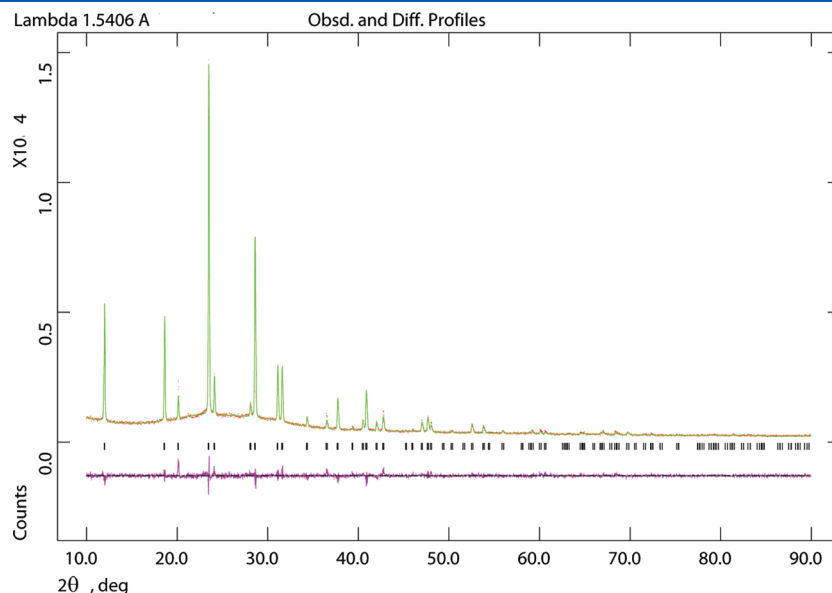


Figure 2. Fitted X-ray powder diffraction pattern obtained at 303 K.

The density of the mixture was 1.01 g/cm³. The sample was rapidly transferred into a cell sealed with Mylar windows. Sample and window thicknesses were 3 mm and 6 μm, respectively. The large-angle X-ray scattering (LAXS) experiments were conducted using the noncommercial energy-scanning diffractometer built in the Department of Chemistry, Rome University “La Sapienza” (Patent n° 01126484 – 23 June 1993, Caminiti R. et al.^{22,23}). White Bremsstrahlung radiation emitted by a tungsten tube operating at 50 kV and 40 mA was used. Scattered intensities for the sample and the empty cell were measured at eight different angles (24.0, 15.5, 8.0, 3.0, 2.0, 1.5, 1.0, and 0.5°). This choice allows covering a wide range of the momentum transfer, Q , namely, between 0.12 and 19.56 Å⁻¹.

The expression for Q is

$$Q = \frac{4\pi \sin \theta}{\lambda} = 1.014E \sin \theta$$

where 2θ is the scattering angle and E is expressed in keV and Q in Å⁻¹. The primary beam intensity $I_0(E)$ was experimentally measured, by reducing the tube current to 10 mA without the sample. Transmission of the sample was measured under the same conditions. Both quantities are needed to carry out the necessary absorption corrections to experimental data. The ultrathin Mylar cell window contribution to the diffraction intensity is less than 1/10 000 of the total. The diffracted intensities recorded at the various angles were normalized to a stoichiometric unit of volume and merged to yield the total static structure factor $I(Q)$, which is given by

$$I(Q) = I_{\text{e.u.}}(Q) - \sum_{i=1}^N x_i f_i^2$$

where $I_{\text{e.u.}}(Q)$ is the observed diffracted intensity in electron units and x_i and f_i are the numerical concentrations of the atoms and their scattering factors. This function was multiplied by Q and by a Q -dependent sharpening factor, $M(Q)$

$$M(Q) = \frac{f_N^2(0)}{f_N^2(Q)} e^{-0.01Q^2}$$

having chosen nitrogen as the sharpening atom. This procedure enhances the resolution of the curve at high Q values and decreases the truncation error in the calculation of the Fourier transform from reciprocal (Q) to direct space (r). The structure function $I(Q)$ has been Fourier-transformed into a radial distribution function ($D(r)$), according to the relation

$$D(r) = 4\pi r^2 \rho_0 + \frac{2r}{\pi} \int_0^{Q_{\max}} Q I(Q) M(Q) \sin(rQ) dQ$$

where ρ_0 is the system density and Q_{\max} is the highest measured Q value (19.56 Å⁻¹).

If the uniform distribution component is dropped, which corresponds to the term $4\pi r^2 \rho_0$, we obtain the differential correlation function, $\text{Diff}(r)$, which contains only the structural contribution to the distribution function. For a detailed discussion of the experimental data treatment, see refs 24–26.

Molecular Dynamics Simulation Details. The MD simulations of the PAC/water mixture were carried out using the DL_POLY package.²⁷ The system was composed by 343 ion pairs and 2233 water molecules (the same molar ratio 1:6.51 used in the experiments) and was placed in a cubic box of 49.4 Å edge, with periodic boundary conditions. The partial charges of the PA

cation were calculated with GAUSSIAN 03²⁸ using the CHELPG procedure²⁹ at the MP2/cc-pVTZ(-f)//HF/6-31G (d) level. All of the other force field parameters for PAC were taken from the Lopes and Padua force field.^{30,31} For water, two of the most widespread water models were employed, namely, the SPC/E⁵ and TIPSP.⁶ The fundamental difference between these models is that while SPC/E is a three-site model with the negative charge on the oxygen atom, TIPSP is a five-site model in which the oxygen is neutral and the negative charge is placed on two massless dummy atoms located orthogonal to the water plane. In the first step of our analysis, two MD simulations were carried out using the SPC/E and TIPSP water models, in which the Lennard-Jones parameters for all of the unlike atoms were obtained from the Lorentz–Berthelot combining rules. In a second step, to improve the description of the experimental data, the two MD simulations with the SPC/E and TIPSP water models have been performed using the same force field parameters with the exception of one Lennard-Jones parameter for the Cl–water interaction ($\sigma_{\text{Cl}-\text{OW}}$), for which the value previously optimized for an EAC/water mixture was used.² The initial configurations were constructed by positioning the ions and the water molecules on selected lattice positions within a very large cubic simulation box. Extensive equilibration runs have been performed, comprising 10 000 steps of initial energy minimization, a short NPT run at 500 K and 10 atm, aimed at randomizing the system followed by another NPT run at 300 K and very high pressure (100 atm) to compress the box volume until the experimental density was reached (1.01 g/cm³). Then the systems have been equilibrated under constant NVT conditions ($T = 300$ K) for about 0.5 ns. The production runs were carried out in the NVT ensemble for 2 ns, with a time step of 1 fs and saving a configuration every 100 time steps. The temperature was kept constant at 300 K using the Nosé–Hoover thermostat^{32,33} with a relaxation constant of 0.5 ps. A cutoff of 8 Å was used to deal with nonbonded interactions, with the Ewald summation method to treat long-range electrostatic effects. All the bonds involving hydrogen atoms were constrained using the SHAKE algorithm.

The theoretical structure factors $I(Q)$ have been calculated from the MD simulations by using the following equation³⁴

$$I(Q) = \sum_{i=1}^N \sum_{j=1}^N x_i x_j f_i f_j H_{ij}(Q)$$

where H_{ij} are the partial structure factors, defined in terms of the radial distribution functions by the Fourier integral

$$H_{ij}(Q) = 4\pi \rho_0 \int_0^{r_{\max}} r^2 (g_{ij}(r) - 1) \frac{\sin(Qr)}{Qr} dr$$

where ρ_0 is the bulk number density of the system and r_{\max} is half the box edge.

The theoretical structure factors have been calculated using in-house written codes. The theoretical $I(Q)$ was then multiplied by Q and by the same sharpening factor used for the experimental data, to obtain a theoretical $QI(Q)M(Q)$ function that can be directly compared with the experimental data. The theoretical $\text{Diff}(r)$ functions were also calculated as described before.

RESULTS AND DISCUSSION

Crystal Polymorphism of PAC. The packing of the LT polymorph of PAC, as determined at RT, is displayed in Figure 3.

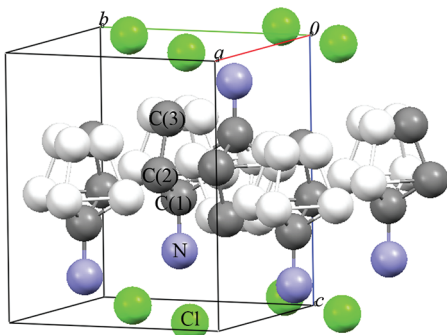


Figure 3. Packing of the LT polymorph of $\text{C}_3\text{H}-\text{NH}_3\text{Cl}$ (Mercury 2.4).³⁵

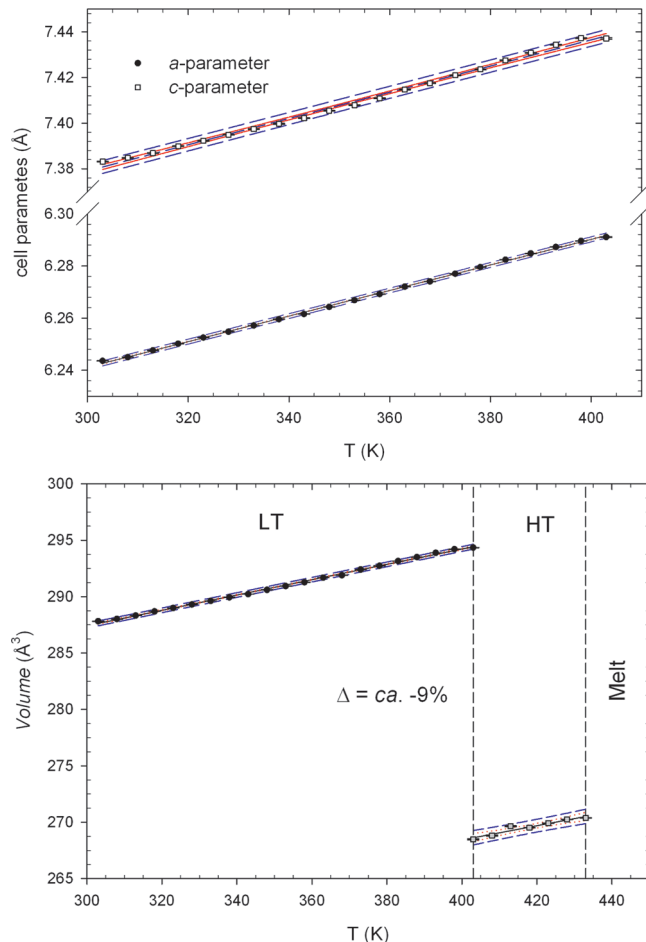


Figure 4. Evolution of cell parameters and volume with temperature: (a) cell parameters; (b) volume.

The Cl^- ions lie in the (001) planes, whereas the propylammonium cation is aligned along the c axis. The $\text{C}(2)$ and $\text{C}(3)$ atoms are rotationally disordered along the $\text{N}-\text{C}(1)$ vector. Figure 3 shows one of the four possible cation configurations (dark gray). Each N atom forms four interactions with Cl^- ions ($\text{N}\cdots\text{Cl}$, ca. 3.23 Å). Such a distance is similar to those observed for the LT polymorph of EAC (3.20–3.25 Å). Evolution of cell parameters and volume with temperature is reported in Figure 4 and the corresponding relative expansion in Figure 5.

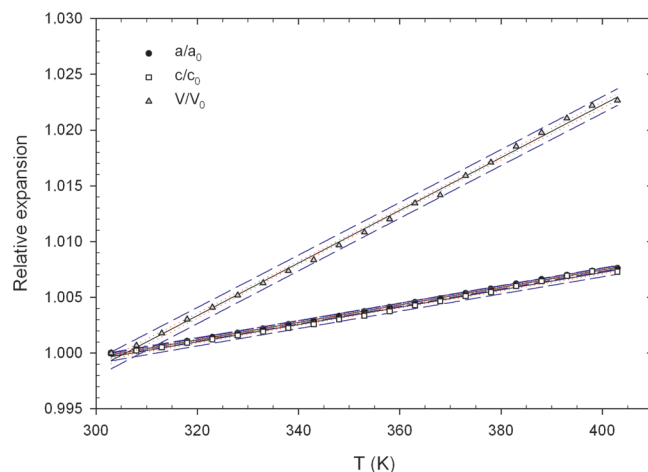


Figure 5. Relative expansion of cell parameters and volume with temperature.

Table 2. Results from the Data-Fitting Procedure Using the Polynomial $p = a_0 + a_1 T$

	a (Å)	c (Å)	volume (Å ³)
R^2	0.9992	0.9954	0.9981
a_0	6.094(1)	7.207(3)	267.0(2)
a_1	$4.90(3) \times 10^{-4}$	$5.74(9) \times 10^{-4}$	$6.80(7) \times 10^{-2}$

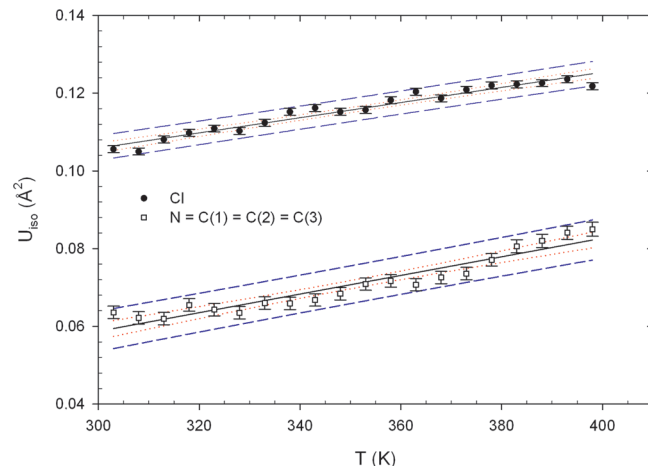


Figure 6. Evolution with temperature of isotropic displacement parameters U_{iso} for the non-hydrogen atoms of the cation and the chlorine ion.

According to the present results, thermal expansion is small and almost perfectly isotropic. Within the investigated thermal range, the volume thermal expansion is of 2.4%. The dependence of the unit cell parameters and volume from temperature have been empirically linearly fitted with the polynomial $p = a_0 + a_1 T$ where a_0 is the value of the corresponding parameter at 0 K; a_1 is the first-order coefficient of expansion; and T is the temperature in K. Results from data fitting are reported in Table 2.

A careful scrutiny of the structural modifications induced by heating reveals that the double sheet behaves as a substantially rigid unit. No variation on intramolecular bond distances as well

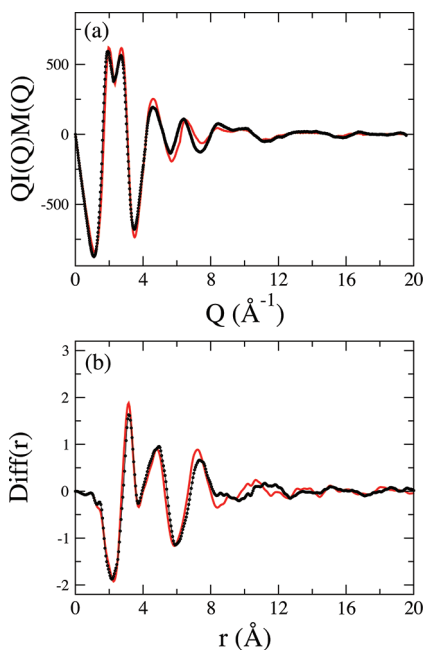


Figure 7. (a) Comparison between the experimental structure factor of the PAC/water mixture (dotted black line) and the experimental structure factor of the EAC/water mixture² (solid red line). (b) Comparison between the experimental $Diff(r)$ function of the PAC/water mixture (dotted black line) and the experimental $Diff(r)$ of the EAC/water mixture² (solid red line).

as very marginal differences in the $N \cdots Cl$ contacts were detected.

Thermal expansion is isotropic as the $N \cdots Cl$ interactions have components along the three crystallographic axes.

As expected, a fairly regular increase of the displacement parameters of both anion and cation atoms is observed throughout the investigated thermal range (Figure 6). The anion has a relatively large isotropic displacement parameter possibly accounting for some positional disorder effect. In effect, moving off-axis the Cl^- ion resulted in a reduction of the corresponding U_{iso} value but at the expense of refinement stability.

For the HT polymorph, 13 peaks were located by a profile-fitting technique using the Topas 4.2 software. Autoindexing was performed using TREOR90.³⁶ A solution was obtained in the cubic system for the following cell parameters, $a = 11.715(3)$ Å and volume = $1607.78(1)$ Å³, and the following figures-of-merit, $M_{13} = 25$ and $F_{13} = 21(0.0219, 29)$.^{37,38} The reported volume is consistent with $Z = 12$. A LeBail fitting carried out with Topas 4.2 pointed out the absence of reflection conditions. Therefore, candidate space groups are $P2_3$, $P\bar{m}\bar{3}$, $P432$, $\bar{P}43m$, and $Pm\bar{3}m$.

According to the symmetry, in this mesophase the cation is expected to perform isotropic rotation, leading to an extended orientational disorder as observed in plastic phases of molecular crystals.^{39,40}

Therefore, no attempt to model such disorder was performed.

It should be noticed that at the transition temperature, the cell volume undergoes a relevant contraction of ca. 9%. Moreover, at the transition temperature and up to melting, an increase of background arising from diffuse scattering occurs. This fact is indicative of the copresence of a highly disordered or amorphous material.

Structural Properties of the PAC/Water Mixture. The experimental X-ray diffraction pattern and $Diff(r)$ function of

the PAC/water mixture are shown as a dotted black line in Figure 7a and b, respectively. The measured $I(Q)$ is characterized by a principal double peak, whose peak positions are found at 1.94 and 2.70 Å⁻¹, followed by two less intense peaks centered at 4.58 and 6.42 Å⁻¹ and some less well-defined oscillations beyond. As far as the $Diff(r)$ function is concerned, three main peaks are found, centered at 3.15 , 4.95 , and 7.35 Å.

It is interesting to compare these patterns with the experimental $I(Q)$ and $Diff(r)$ functions previously obtained for a mixture of EAC and water using the same ion concentration.² As can be seen from Figure 7a, the $I(Q)$'s for the PAC/water and EAC/water mixtures are very similar, and only slight differences between the two X-ray diffraction patterns are found in the Q range between 5 and 9 Å⁻¹. The observed differences can be better interpreted from the comparison of the $Diff(r)$ functions in distance space (see Figure 7b). The PAC and EAC $Diff(r)$'s show a very similar trend. In particular, they are almost identical in the distance region of the first and second peak, while the third peak is slightly shifted toward shorter distances and has a higher intensity in the EAC/water mixture, as compared to the PAC/water one. These results indicate that the local structure in a range of about 6 Å is very similar in both systems, while the mixture with EAC shows a slightly higher degree of long-range structuring than the mixture containing PAC.

To interpret the X-ray diffraction data of the PAC/water mixture, we have carried out two MD simulations of the system with the SPC/E and TIPSP water models, by using the force field parameters reported in the literature and obtaining the Lennard-Jones parameters for all of the unlike atoms from the Lorentz–Berthelot combining rules (see Methods section). The comparisons between the experimental structure factor $I(Q)$ and the theoretical ones calculated from the two MD simulations are shown in Figure 8a and 8b. As far as the SPC/E water model is concerned, the agreement between the theoretical and experimental $I(Q)$'s is not good, especially in the range between 4 and 12 Å⁻¹ where the theoretical peaks are shifted toward larger Q values and have a higher intensity as compared to the experimental ones. Even if a better agreement between theory and experiment is found with the TIPSP water model, also in this case the experimental pattern of peak positions and intensities is not correctly reproduced. To clarify the origin of these discrepancies, it is extremely useful to compare the theoretical and experimental $Diff(r)$ functions in distance space (Figure 8c and 8d). Noticeable differences can be observed in all the distance ranges for both the SPC/E and TIPSP simulations. In particular, for the SPC/E water model, the theoretical second peak is too high and shifted toward shorter distances, and the third peak shows a different trend in the region between 8.3 and 9.6 Å, as compared to the experimental one. In the case of the TIPSP simulation, the third peak is significantly less intense, and it is positioned at distances shorter than the experimental results. Moreover, large discrepancies between theory and experiment are found in the first peak region. In particular, the positions of the theoretical first peaks are shifted toward shorter distances (2.95 and 3.05 Å for the SPC/E and TIPSP water model, respectively), and the intensities are much higher than the experimental one, especially in the SPC/E calculation.

Due to the strong anion–water interactions, to the large scattering factor of chlorine, and to the large number of water molecules present in the mixture, the main contributions to the first peak originate from contacts between the chloride ion and the oxygen atoms of water molecules belonging to the Cl^- first

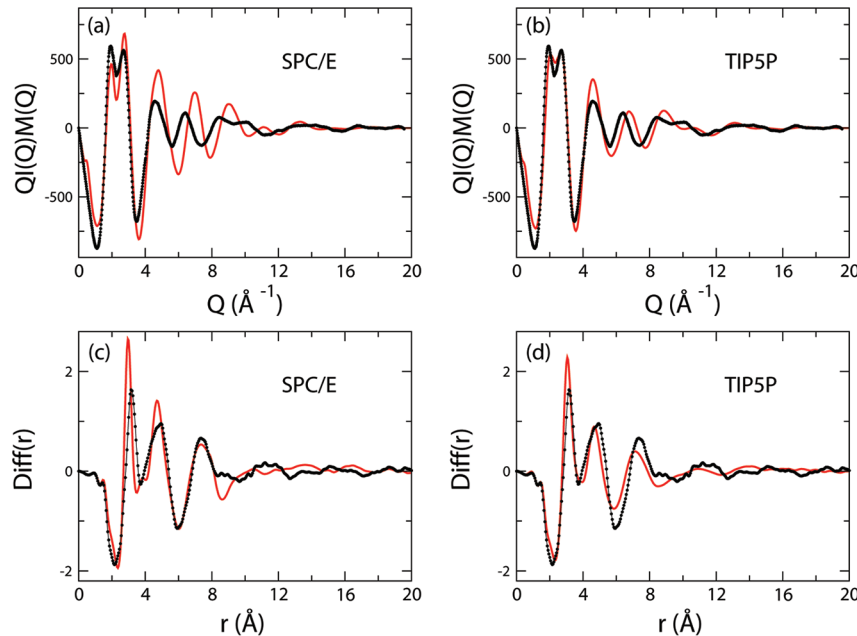


Figure 8. Comparison between the experimental structure factor (dotted black line) and the theoretical one (solid red line) calculated from the SPC/E (a) and TIP5P (b) trajectories. Comparison between the experimental $\text{Diff}(r)$ function (dotted black line) and the theoretical one (solid red line) calculated from the SPC/E (c) and TIP5P (d) trajectories. The MD simulations were carried out using Lennard-Jones parameters for all of the unlike atoms obtained from the Lorentz–Berthelot combining rules.

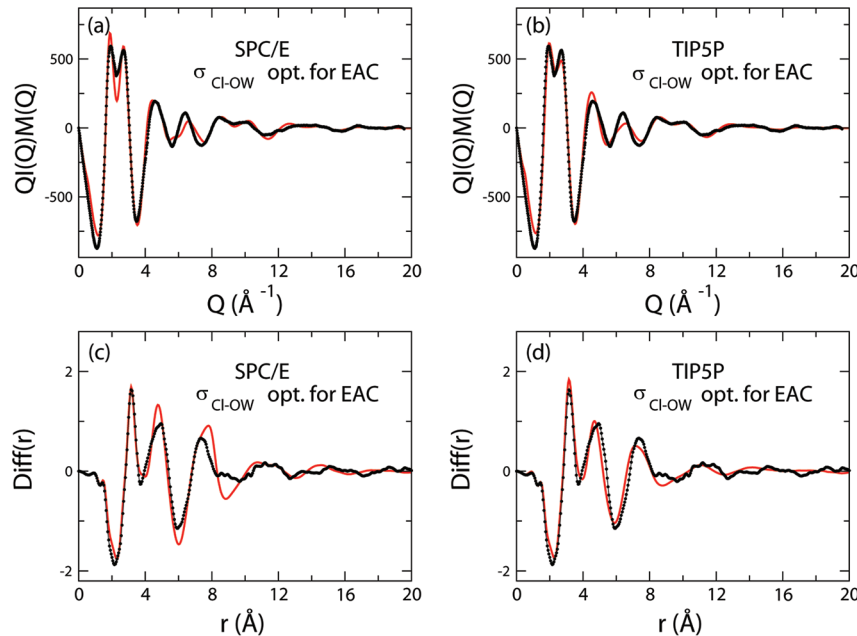


Figure 9. Comparison between the experimental structure factor (dotted black line) and the theoretical one (solid red line) calculated from the SPC/E (a) and TIP5P (b) trajectories. Comparison between the experimental $\text{Diff}(r)$ function (dotted black line) and the theoretical one (solid red line) calculated from the SPC/E (c) and TIP5P (d) trajectories. The MD simulations were carried out using Lennard-Jones parameters for all of the unlike atoms obtained from the Lorentz–Berthelot combining rules with the exception of the $\sigma_{\text{Cl-OW}}$ parameter for the Cl–water interaction for which the value previously optimized for an EAC/water mixture was used.²

coordination sphere and from oxygen–oxygen interactions between nearest-neighbor water molecules.

Since the Lennard-Jones parameters for cross interactions in a mixture do not necessarily follow any simple set of “mixing rules”, the disagreement between the theoretical and experimental

$\text{Diff}(r)$ first peak points to the need of improving the description of the chloride–water cross interactions.

As previously mentioned, in a recent work we have investigated the structural properties of an EAC/water mixture by combining MD simulations and X-ray diffraction experiments,

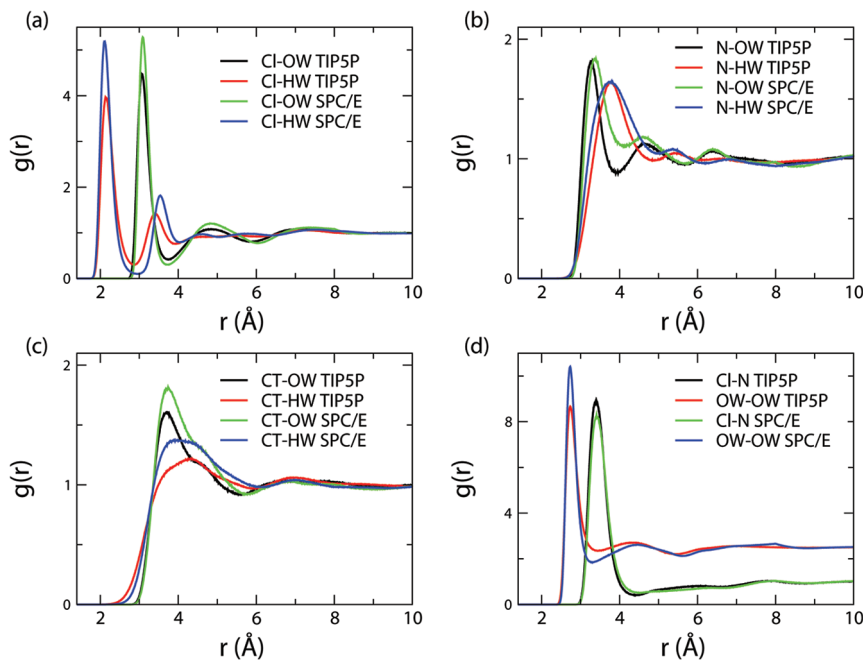


Figure 10. Radial distribution functions $g(r)$'s of a selected subset of atoms calculated from the SPC/E and TIP5P simulations. OW and HW are the oxygen and hydrogen atoms of the water molecules, while CT is the C atom of the terminal methyl group. The OW–OW $g(r)$'s are shown multiplied by a factor of 2.5 for clarity.

Table 3. Structural Parameters of the Radial Distribution Functions $g(r)$'s Depicted in Figure 10^a

	R (Å)	N	cutoff distance (Å)
Cl–OW SPC/E	3.09	4.20	3.70
Cl–OW TIP5P	3.08	4.17	3.76
N–OW SPC/E	3.37	4.50	4.10
N–OW TIP5P	3.27	3.50	3.93
CT–OW SPC/E	3.74	14.73	5.70
CT–OW TIP5P	3.72	12.90	5.62
Cl–N SPC/E	3.41	2.18	4.45
Cl–N TIP5P	3.40	2.17	4.41
OW–OW SPC/E	2.74	2.87	3.30
OW–OW TIP5P	2.74	3.20	3.40

^a R is the position of the $g(r)$ first peak, and N is the coordination number calculated by integration of the $g(r)$. The cutoff distances used in the calculation of N are also reported.

and with the aim of providing a reliable description of the system, we optimized a single force field parameter, namely, the σ parameter of the Cl–OW (OW is the oxygen atom of the water molecule) Lennard-Jones potential, until the best possible agreement between the MD results and the experimental data was reached.²

Here, to improve the agreement between theory and experiment, we have resorted to using the $\sigma_{\text{Cl}-\text{OW}}$ parameter previously optimized for the EAC/water mixture, to describe the chloride–water interactions also in the present system.

By employing the previously refined $\sigma_{\text{Cl}-\text{OW}}$ value, a much better agreement between the theoretical and experimental $I(Q)$'s was found for both water models (Figure 9a and 9b). As far as the $\text{Diff}(r)$ functions are concerned, the position of the experimental first peak at 3.15 Å is perfectly reproduced by the

two MD simulations carried out with the optimized $\sigma_{\text{Cl}-\text{OW}}$ values (Figure 9c and 9d). In the distance region of the first peak, the theoretical SPC/E and TIP5P $\text{Diff}(r)$'s match the experimental data very well, meaning that the local contacts among all of the atoms in the system in a range of about 4 Å are correctly reproduced by both water models. A different result has been obtained for the long-range interactions. As it can be seen, for distances larger than 4 Å, the theoretical $\text{Diff}(r)$ calculated from the TIP5P simulation is in much better agreement with the experimental data, as compared to the SPC/E case, thus showing that the TIP5P water model provides a better description of the long-range structure formed in the PAC/water mixture. This is in line with the results previously obtained for the EAC/water system.² Interestingly, by lengthening the alkyl chain of the cation from ethyl to propyl, the better performance of the TIP5P water model as compared to the SPC/E one becomes more evident. For the EAC/water system, indeed the distance region of the $\text{Diff}(r)$ second peak was correctly reproduced also by the SPC/E simulation,² while for PAC also in this region the TIP5P results are in better agreement with the experiment.

It is noteworthy that such a good agreement between theory and experiment has been obtained by using a $\sigma_{\text{Cl}-\text{OW}}$ parameter not specifically optimized for the present system but refined for the EAC/water one.

Several attempts have been made to further optimize $\sigma_{\text{Cl}-\text{OW}}$ for both the SPC/E and TIP5P simulations to improve the agreement between the theoretical and experimental diffraction patterns, but in all cases we obtained a worse agreement with the experimental data.

To have an idea of the sensitivity of the obtained theoretical $\text{Diff}(r)$ functions to the $\sigma_{\text{Cl}-\text{OW}}$ value, note that a decrease/increase of only 0.02 Å of the $\sigma_{\text{Cl}-\text{OW}}$ refined for the TIP5P water model resulted in a shift of the TIP5P $\text{Diff}(r)$ first peak to

3.10/3.20 Å, which is a shift of about 0.05 Å as compared to the experimental peak position.

To gain an overall view of the structural properties of the PAC/water mixture, we have calculated the radial distribution functions $g(r)$'s of a selected subset of atoms. All of the calculated $g(r)$'s are depicted in Figure 10, and selected first peak positions are reported in Table 3. We refer to the oxygen and hydrogen atoms of the water molecule as OW and HW. The Cl–OW and Cl–HW $g(r)$'s calculated from the SPC/E and TIPSP simulations (Figure 10a) show very sharp and distinct first peaks, indicating that strong anion–water interactions are present, in agreement with prevailing concepts.⁴¹ Moreover, in the Cl–HW $g(r)$'s, two peaks are found, the former at shorter distances and the latter at longer distances as compared to the Cl–OW $g(r)$ first maxima, and this means that the first shell water molecules orient only one hydrogen atom toward Cl^- , as also shown for other halide ions in aqueous solution.⁴² This is in line with the strong ability of the Cl^- ion to form hydrogen bonds. As concerns the differences between the two water models, the positions of the Cl–OW and Cl–HW $g(r)$ first peaks are very similar in both trajectories, while their intensities are higher in the SPC/E simulation, indicating a more structured Cl^- first coordination sphere. The N–OW and N–HW $g(r)$'s (Figure 10b) show the existence of a first hydration shell also around the N atom of the cation, but the peaks are less pronounced as compared to the Cl–water $g(r)$'s, as a consequence of weaker cation–water interactions as compared to the anion–water ones. The first shell water molecules on average prefer to orient the oxygen toward the N atom, but the oxygen and hydrogen $g(r)$ first peaks are not well separated, and a larger orientational freedom is found, as compared to the chloride first hydration shell. As far as the carbon atom of the terminal methyl group is concerned (CT), the positions of the CT–OW and CT–HW $g(r)$ first peaks are quite similar (Figure 10c), thus suggesting an almost tangential arrangement of water molecules in the vicinity of the methyl group. Even if the water molecules strongly interact with Cl^- and to a lesser extent with PA, cations and anions are not completely separated, as shown by the strong Cl–N correlation that is found in both the SPC/E and TIPSP simulations (Figure 10d). Moreover, the high and well-defined short-range peak of the OW–OW $g(r)$ (Figure 10d) suggests that the water molecules in the mixture tend to aggregate and form water clusters.

To better quantify the structural features of the PAC/water system, we have computed a series of coordination numbers. These represent the average number of atoms within a given cutoff distance from the selected reference atom, and they are obtained by the numerical integration of the radial distribution function. For each selected couple of atoms, the cutoff distance has been chosen as the position of the first minimum of the corresponding radial distribution function. The coordination numbers obtained from the two simulations are reported in Table 3, together with the cutoff distances used in the calculations.

In both the SPC/E and TIPSP simulations the first hydration shell of chloride contains about 4.2 water molecules. This coordination number is lower than the hydration number of chloride in aqueous solution, which is 6 according to most X-ray and neutron diffraction studies,^{43–46} but is similar to the number of water molecules (4.75) that have been found in the Cl^- first hydration shell in a recent Car–Parrinello simulation of one 1-ethyl-3-methylimidazolium chloride ion pair dissolved in 60 water

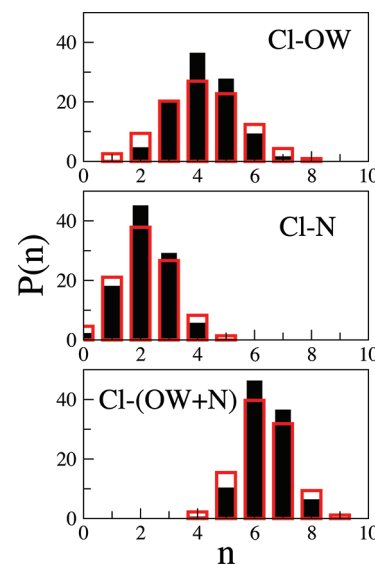


Figure 11. Distributions of the Cl^- instantaneous coordination number (n) calculated for the oxygen atom of the water molecules (Cl–OW), for the N atom of the cations (Cl–N), and for the sum of the oxygen and nitrogen atoms (Cl–(OW + N)). The results obtained from the SPC/E simulation are shown as full black bars and the TIPSP ones as empty red bars.

molecules.⁴⁷ Moreover, the Cl–OW coordination number is slightly lower than the same hydration number calculated for the EAC/water mixture (4.5), and this can be due to the fact that the number of water molecules is slightly lower in the PAC/water system as compared to the EAC/water one.² Even if over a larger distance range, a similar number of water molecules are present also in the first coordination shell of the N atom (in the TIPSP case, this number is lower), while a huge hydration number is obtained for the CT atom, which is due to the very large cutoff distance used in the calculation. The water–water coordination number is 3.2 in the TIPSP simulation and slightly lower in the SPC/E one, while both the SPC/E and TIPSP trajectories predict the presence of about 2.2 cations in the first coordination shell of the anion and vice versa. Note that all of the coordination numbers involving the OW atom are slightly lower than the corresponding ones previously calculated from the simulation of the EAC/water mixture,² as a consequence of the slightly lower water concentration in the PAC/water system.

A careful analysis of the SPC/E and TIPSP simulations has highlighted that cation and anion do not possess a completely closed hydration shell of their own, but rather “solvent-shared ion pairs” are formed, in which one or more water molecules belonging to the first solvation shell of the anion can act as a bridge and thus be shared with the N atom of the cation. In this complex network of interactions, a quantitative insight into the local environment seen by the Cl^- ion can be gained by defining an instantaneous coordination number n of Cl^- as the number of atoms of a certain type (X) at a distance from chloride shorter than the $\text{Cl}-\text{X}g(r)$ first minimum (see Table 3) and analyzing its variation along the simulations.

In particular, we have calculated the coordination number distributions for the oxygen atom of the water molecules, for the N atom of the cations, and for the sum of the oxygen and nitrogen atoms (see Figure 11). The results of this analysis show that in both trajectories the Cl^- ion transits among several Cl–O and

Cl–N coordination numbers, and the distributions obtained from the TIPSP simulation are broader than the SPC/E ones. However, for both water models we have found a dominant percentage of the Cl[−] first coordination shell containing six first neighbors, i.e., four water molecules and two N atoms of the cation. Moreover, the percentage of Cl[−] local environments with no N atoms within the cutoff distance is very low (below 5%) in both simulations.

Altogether, our results show that the structural properties of the PAC/water mixture are very similar to those previously found for the EAC/water one.² In both systems, the intruding water does not break up the cation–anion network so that solvent shared ion pairs are formed, while the water molecules tend to aggregate and form water clusters especially in the neighborhood of the CT atom of the cation.

CONCLUSIONS

The thermal behavior of propylammonium chloride has been investigated by parallel beam X-ray powder diffraction in the 303–463 K thermal range. A polymorphic transition has been observed at 403 K. The melting process occurred at 438 K. The low-temperature (LT) polymorph is tetragonal, $P4/n$ or $P4/nmm$, with $a = 6.2429(2)$ Å, $c = 7.3830(3)$ Å, and $Z = 2$. Thermal expansion is isotropic, and the volume expansion is ca. 2.4% in the investigated thermal range. The isotropy has been attributed to the fact that the N···Cl interactions have components along the three crystallographic axes. At the transition temperature, a high-temperature (HT) polymorph was observed. The absence of extinction rules pointed out to $P2_1$, $Pm\bar{3}$, $P432$, $\bar{P}43m$, and $Pm\bar{3}m$ as candidate space groups, with cell parameter $a = 11.715(3)$ Å, consistent with $Z = 12$. Due to the high symmetry, the HT phase is expected to show extended orientational disorder, similarly to plastic phases of molecular crystals.

The structural properties of a PAC/water mixture have been investigated by combining MD simulations and X-ray diffraction experiments. Two of the most widespread water models, namely, the SPC/E and TIPSP, were used in the calculations, while for PAC the Lopes–Padua force field was employed. The use of the $\sigma_{\text{Cl}-\text{OW}}$ Lennard-Jones parameter previously refined to obtain the best possible agreement between the MD structural results and the X-ray diffraction experimental data of an EAC/water mixture has allowed us to obtain here a very good agreement between the theoretical and experimental diffraction patterns of the PAC/water mixture. This is a very important result indicating that the $\sigma_{\text{Cl}-\text{OW}}$ Lennard-Jones parameter previously optimized is transferable between the two studied systems. Transferability of the functional form and parameters is an important feature of a force field as it means that the same set of parameters can be used to model a series of related molecules rather than having to define a new set of parameters for each individual molecule. We are currently extending and validating the present set of force field parameters for mixtures with water of alkylammonium chlorides with longer alkyl chains, such as hexylammonium chloride and decylammonium chloride, and in different conditions of water concentration, and this will be the subject of a future paper.

We have found that the results of the TIPSP simulation were in much better agreement with the experimental data, as compared to the SPC/E case, thus showing that the TIPSP water model provides a better description of the structure formed in the PAC/water mixture. Interestingly, the better performance of the TIPSP water model as compared to the SPC/E one becomes

more evident when the alkyl chain of the cation is lengthened from ethyl to propyl.

The structural properties of the PAC/water mixture have been found to be very similar to those previously found for the EAC/water one.² A complex structural behavior emerged from the analysis of the trajectories, in which cations and anions form solvent-shared ion pairs: the chloride ion is surrounded on average by four water molecules and two cations, and one or more water molecules act as a bridge between the anion and the cations.

ASSOCIATED CONTENT

S Supporting Information. CIF files of the refinements carried out at the various temperatures are available as Supporting Information. This material is available free of charge via the Internet at <http://pubs.acs.org>.

AUTHOR INFORMATION

Corresponding Author

*E-mail: paolo.ballirano@uniroma1.it.

ACKNOWLEDGMENT

This work was supported by the University of Rome La Sapienza (Progetto Protic Ionic Liquids, ateneo 2010). Moreover it was supported by CASPUR with the Standard HPC Grant 2011 entitled: “Protic ionic liquids”. L.G. acknowledges support from the FIRB “Futuro in Ricerca” research project (RBFR086BOQ_001, “Structure and dynamics of ionic liquids”). V.M. wishes to thank Dr. Enrico Bodo for his fundamental contribution to the development of the codes to calculate the theoretical X-ray structure factors.

REFERENCES

- (1) Zabinska, G.; Drozdowska, G.; Kisza, A. *J. Chem. Eng. Data* **1998**, *43*, 562.
- (2) Migliorati, V.; Ballirano, P.; Gontrani, L.; Triolo, A.; Caminiti, R. *J. Phys. Chem. B* **2011**, *115*, 4887.
- (3) King, M. V.; Lipscomb, W. N. *Acta Crystallogr.* **1950**, *3*, 222.
- (4) King, M. V.; Lipscomb, W. N. *Acta Crystallogr.* **1950**, *3*, 227.
- (5) Berendsen, H. J. C.; Grigera, J. R.; Straatsma, T. P. *J. Phys. Chem.* **1987**, *91*, 6269.
- (6) Mahoney, M. W.; Jorgensen, W. L. *J. Chem. Phys.* **2000**, *112*, 8910.
- (7) Ballirano, P.; Melis, E. *Phys. Chem. Miner.* **2007**, *34*, 699.
- (8) Ballirano, P.; Melis, E. *Phys. Chem. Miner.* **2009**, *36*, 319.
- (9) Ballirano, P.; Melis, E. *Phys. Chem. Miner.* **2009**, *36*, 391.
- (10) Ballirano, P.; Sadun, C. *Struct. Chem.* **2009**, *20*, 815.
- (11) Ballirano, P.; Caminiti, R. *J. Phys. Chem. A* **2009**, *113*, 7774.
- (12) Bruker AXS Topas V4.2: General profile and structure analysis software for powder diffraction data; Bruker AXS: Karlsruhe, Germany, 2009.
- (13) Altomare, A.; Burla, M. C.; Camalli, M.; Carrozzini, B.; Casciarano, G.; Giacovazzo, C.; Guagliardi, A.; Moliterni, A. G. G.; Polidori, G.; Rizzi, R. *J. Appl. Crystallogr.* **1999**, *32*, 339.
- (14) Altomare, A.; Burla, M. C.; Camalli, M.; Casciarano, G.; Giacovazzo, C.; Guagliardi, A.; Moliterni, A. G. G.; Polidori, G.; Spagna, R. *J. Appl. Crystallogr.* **1999**, *32*, 115.
- (15) Larson, A. C.; Von Dreele, R. B. GSAS General Structure Analysis System. LAUR 86–748, Los Alamos National Laboratory. The Regents of the University of California, 2000.
- (16) Toby, B. H. *J. Appl. Crystallogr.* **2001**, *34*, 210.

- (17) Thompson, P.; Cox, D. E.; Hastings, J. B. *J. Appl. Crystallogr.* **1987**, *20*, 79.
- (18) Finger, L. W.; Cox, D. E.; Jephcoat, A. P. *J. Appl. Crystallogr.* **1994**, *27*, 892.
- (19) Baerlocher, C. H. Restraints and constraints in Rietveld refinement. In *The Rietveld method*; Young, R. A., Ed.; Oxford Science: Oxford, 1993; Chapter 10.
- (20) Von Dreele, R. B. *J. Appl. Crystallogr.* **1997**, *30*, 517.
- (21) Young, R. A. Introduction to the Rietveld method. In *The Rietveld method*; Young, R. A., Ed.; Oxford Science: Oxford, 1993; pp 1–38.
- (22) Caminiti, R.; Sadun, C.; Rossi, V.; Cilloco, F.; Felici, R. Italian Patent No. 01261484 23 June 1993.
- (23) Rossi Albertini, V.; Bencivenni, L.; Caminiti, R.; Cilloco, F.; Sadun, C. *J. Macromol. Sci. Phys. B* **1996**, *35*, 199.
- (24) Atzei, D.; Ferri, T.; Sadun, C.; Sangiorgio, P.; Caminiti, R. *J. Am. Chem. Soc.* **2001**, *123*, 2552.
- (25) Carbone, M.; Caminiti, R.; Sadun, C. *J. Mater. Chem.* **1996**, *6*, 1709.
- (26) Abis, L.; Dell'Amico, D. B.; Busetto, C.; Calderazzo, F.; Caminiti, R.; Ciolfi, C.; Garbassi, F.; Mascarelli, G. *J. Mater. Chem.* **1998**, *8*, 751.
- (27) Smith, W.; Forester, T. *J. Mol. Graphics* **1996**, *14*, 136.
- (28) Frisch, M. J. et al. *Gaussian 03*, revision C.02; Gaussian, Inc.: Wallingford CT, 2004.
- (29) Breneman, C. M.; Wiberg, K. B. *J. Comput. Chem.* **1990**, *11*, 361.
- (30) Canongia Lopes, J. N.; Pádua, A. A. H. *J. Phys. Chem. B* **2004**, *108*, 16893.
- (31) Canongia Lopes, J. N.; Deschamps, J.; Pádua, A. A. H. *J. Phys. Chem. B* **2004**, *108*, 2038.
- (32) Evans, D. J.; Holian, B. L. *J. Chem. Phys.* **1985**, *83*, 4069.
- (33) Nosé, S. *J. Chem. Phys.* **1984**, *81*, 511.
- (34) Pings, C. J.; Waser, J. *J. Chem. Phys.* **1968**, *48*, 3016.
- (35) CCDC. *Mercury 2.4*; Cambridge Crystallographic Data Centre: 12 Union Road, Cambridge, England, 2002.
- (36) Werner, P. E.; Eriksson, L.; Westdahl, M. *J. Appl. Crystallogr.* **1985**, *18*, 367.
- (37) de Wolff, P. M. *J. Appl. Crystallogr.* **1968**, *1*, 108.
- (38) Smith, G. S.; Snyder, R. L. *J. Appl. Crystallogr.* **1979**, *12*, 60.
- (39) Sherwood, J. N. *The plastically crystalline state*; Wiley: New York, 1979.
- (40) Chezeau, J. M.; Strange, J. H. *Phys. Rep.* **1979**, *53*, 1.
- (41) Cammarata, L.; Kazarian, S. G.; Salter, P. A.; Welton, T. *Phys. Chem. Chem. Phys.* **2001**, *3*, 5192.
- (42) D'Angelo, P.; Migliorati, V.; Guidoni, L. *Inorg. Chem.* **2010**, *49*, 4224.
- (43) Caminiti, R.; Licheri, G.; Piccaluga, G.; Pinna, G.; Radnai, T. *J. Chem. Phys.* **1979**, *71*, 2473.
- (44) Caminiti, R.; Licheri, G.; Paschina, G.; Piccaluga, G.; Pinna, G. *Z. Naturforsch.* **1980**, *35a*, 1361.
- (45) Caminiti, R.; Musinu, A.; Paschina, G.; Pinna, G. *J. Appl. Crystallogr.* **1982**, *15*, 482.
- (46) Ohtaki, H.; Radnai, T. *Chem. Rev.* **1993**, *93*, 1157.
- (47) Spickermann, C.; Thar, J.; Lehmann, S. B. C.; Zahn, S.; Hunger, J.; Buchner, R.; Hunt, P. A.; Welton, T.; Kirchner, B. *J. Chem. Phys.* **2008**, *129*, 104505.